Available online at www.sciencedirect.com
SCIENCE DIRECT
Journal of Power Sources 157 (2006) 550–562
JOURNAL OF POWER SOURCES
www.elsevier.com/locate/jpowsour

Influence of the nonionic surfactant Triton X-100 on electrocrystallization and electrochemical performance of lead dioxide electrode

M. Ghaemi [a,*], E. Ghafouri [a], J. Neshati [b]

[a] *Department of Chemistry, School of Sciences, Tarbiat Modarres University, P.O. Box 14115-175, Tehran, Iran*
[b] *Corrosion department, Research Institute of Petroleum Industry, Tehran, Iran*

Received 9 June 2005; accepted 28 July 2005
Available online 25 October 2005

Abstract

Effects of the nonionic t-octyl phenoxy polyethoxyethanol (Triton X-100) on electrocrystallization of lead dioxide were investigated on titanium substrates in the bath containing nitric acid solutions and lead nitrate. Two series of samples were produced in the presence (modified samples: PTX) and in the absence of Triton X-100 (unmodified samples: PT) at bath temperatures ranging from 25–100 °C. Higher current efficiencies, mechanical strength and more adhesion to Ti substrates were found for modified samples. Results confirm an increase in the overpotential for oxygen evolution during electrodeposition process in the presence of Triton X-100. It is suggested that the accumulation of oxygen species and the growth of crystals could be affected through the aqueous network of the self-assembled surfactants on the electrode surface. A higher overpotential for oxygen evolution reaction was also observed for electrodes made of PTX samples in sulfuric acid solution. Results of the voltammetric experiments and those from laboratory-designed test cells have confirmed a higher charge/discharge performance of modified samples towards the $PbO_2/PbSO_4$ transformation in aqueous sulfuric acid solutions.

Scanning electron microscopy (SEM) has shown reduced morphological defects of PTX samples at all bath temperatures. This was in agreement with X-ray diffractograms, showing more crystalline appearance and regularity, compared to those of unmodified samples. The sample obtained under optimized conditions (synthesis in the presence of Triton X-100 at a bath temperature around 100 °C), had a higher degree of crystallinity and electrochemical activity. The enhanced characteristics of this sample is attributed to its special morphology due to creation of large number of small micropores, strong incorporation of hydrogen species and enhanced proton diffusivity as confirmed by SEM, thermogravimmetric analysis (TGA) and Electrochemical Impedance Spectroscopy (EIS).

Keywords: Lead dioxide; PbO_2; Lead acid batteries; Bipolar; Surfactant; Electrodeposition

1. Introduction

Discharge performances of lead/acid batteries are mainly limited by the positive plate and the related aging mechanism, which are often inter-dependent [1]. For example, PbO_2 degradation could cause irreversible formation of lead sulfate in the active mass, short-circuits and grid corrosion processes. These could lower the conductivity, homogeneity of the current distribution and the average mass utilization [2]. Premature capacity loss (PCL) is mainly related to degradation of positive active material (PAM) leading to disruption of the connections between PbO_2 particles and deactivation of active material (shedding or slugging). At the same time, a loss of mechanical and electronic contact between grid and active material could be expected [3]. In addition, higher molar volumes of discharge products and swelling of active mass lead to degradation of microstructure of PAM. It is reported that the maximum real utilization rate is 55% [4] or even lower for lead dioxide electrode. Even though these active materials are not discharged, they must still provide structure and conductivity.

In an attempt to reduce the active mass degradation and evaluate its physico-chemical characteristics, we report on the electrodeposition of PbO_2 from nitric acid solutions conditioned by the nonionic surfactant Triton X-100 (abbreviated as TX100, Merck). Interest may be focused, for example, on control of surface hydroxyl-radicals through hindering or promoting water discharge at the electrode/solution interface [5], which plays an important role in many areas of technology. Hence, the hydration

* Corresponding author. Tel.: +98 21 801 1001/4412; fax: +98 21 800 9730.
E-mail address: ghaemi_m@modares.ac.ir (M. Ghaemi).

0378-7753/$ – see front matter © 2005 Elsevier B.V. All rights reserved.
doi:10.1016/j.jpowsour.2005.07.089

degree of the surface seems to be an important parameter whose control can affect the efficiency of several oxidation processes relative to O_2 generation [45]. An increase in overpotential for oxygen evolution is very important in oxidation carried out at high anodic potentials, because the evolution of O_2 can lower the current efficiency of the main processes [6]. Generally, Oxygen evolution could promote breaking and resistivity of the positive active material [7].

Valuable investigations have been carried out to suppress the onset of gassing by using additives [8,9]. A number of organic additives such as sodium lauryl sulphate [10], sodium dodecyl sulphonate (SDS), gelatin, dextrin [11] and nicotinamide [12] were used for enhancement of lead acid batteries. The effect of inorganic additives such as H_3PO_4 [13,14] and metal sulfates [15–17] was also studied extensively to optimize the cycle performance of lead dioxide.

Electrodeposition from homogeneous mixture of self-assembled monolayer of surfactants systems has been published in recent years in electrochemical literature. The well-defined microstructures of surfactant molecules formed on the electrode surface could serve as templates for the electrochemical process [18–20]. In this relation, nanoporous materials have been produced using concentrated surfactant solutions as liquid crystalline templates [21–23]. In our earlier work [24], we showed that dilute solutions of surface active agents had influence on the electrochemical kinetics of Manganese dioxide.

The purpose of this work is to investigate and develop the anodically grown PbO_2 in the presence of TX100 and its characterization. The mechanism of TX100 actions have been studied and discussed in this paper. We also discussed the electrochemical data obtained from modified and unmodified samples based on electrodeposition conditions and electrochemical characterizations. In addition to examining the role of TX100, we also intended to check on the influence of bath temperature on the electrochemical behavior of resulting oxide. One reason for this choice is the influence of both surfactant and bath temperature on most interface process including electrokinetics and oxygen evolution [24–25].

The low utilization efficiency of the active mass, especially on positive electrode, limits the actual specific energy of the lead–acid battery [26]. The use of thin plates is probably a very important way to reduce the battery dead weight and decrease the ohmic losses between positive and negative active materials [27]. As a result, active materials work more homogeneously. In Bipolar lead/acid batteries, conventional plates is replacing with thin layers of electroactive materials. Besides, it is advantageous to have as light a collector as possible in accordance to environmentally more acceptable reduction of polluting nature of lead and its compounds [28–30]. Use of structures based on lightweight electronically conducting polymers could lead to significant improvements of the battery performance. In addition, the current collector structure must allow for significant volume increase during discharge, while maintaining sufficient electrical contact with the active material particles [31]. Other important factors are effective grid surface area in relation to PAM weight [32] and the maximum current density of the current collector [33]. In this paper, we report on preliminary investigation for the application of conductive polyethylene foil coated with thin layers of graphite as current collectors [34] to meet this requirement. We wish to address the question whether or not these polymer substrates are applicable in bipolar designs.

2. Experimental

2.1. Material synthesis, characterization, and electrochemical test procedures

Electrosynthesis of PbO_2 was performed at anodic current densities of $\leq 1\ A\ dm^{-2}$ during 36 h electrolysis using a laboratory scale electrolyzer in the bath containing standard electrolyte consisting of lead nitrate (0.5 M) and nitric acid (0.1 M). Detailed descriptions of the construction of electrolyzer can be found in our previous work [35]. Two series of PbO_2 samples were prepared in the presence (PTX samples) and absence of surfactants (PT samples) at different bath temperatures. All PTX samples were prepared by adding same quantity of TX100 (0.3 wt.%) directly into the aqueous electrolyte. The critical micelle concentration (cmc) value of TX100, is equal to 3.0×10^{-4} M (0.02 wt.%) [24].

Electrolyte solutions with bath temperatures of 25, 50, 75 and $100 \pm 3\ ^\circ C$ were prepared in the presence of TX100 and the resulting PbO_2 samples have been labeled as PTX25, PTX50, PTX75 and PTX100. PbO_2 Samples prepared under the same bath conditions but in the absence of surfactant, have been labeled as PT25, PT50 and PT75. PT100 could not be prepared in our experimental conditions probably because of strong passivation of Ti substrate. Deposited PbO_2 layers were mechanically removed, rinsed with distilled water and ground with a pestle and mortar. Subsequently, the samples were dried and then sieved through 300 μm mesh screen for use in test cells, thermogravimetric analysis (TGA) and X ray diffraction spectroscopy (XRD). Thin layers of PbO_2 scraped off the anode, washed thoroughly with distilled water, and dried in air for further study of surface morphologies.

Microscopic characterization of all modified and unmodified PbO_2 samples were performed by means of scanning electron microscopy (SEM) (Philips XL 30). Thermal gravimetric analysis of obtained materials were carried out by means of PL-STA1500, at a ramp rate of $10\ ^\circ C\ min^{-1}$. Powder X-ray diffraction, was used to study further characterizations, changes in crystallinity and phase transformation of PbO_2. XRD patterns were recorded by using a Philips Xpert diffractometer and Cu Kα radiation ($\lambda = 0.15418$ nm).

Electrochemical impedance spectroscopy (EIS) measurements were performed by using a working electrode coated with thin layer of PbO_2 electrodes. These electrodes were prepared via electrodeposition on Ti substrates for 28 min using standard bath. EIS tests were carried out in sulfuric acid 1 M, in the range of 100 kHz and 100 mHz, at open circuit voltage (OCV) and ±5 mV potential amplitude. The impedance data was acquired and analyzed by the computer software Z-view from a Solartron 1255 frequency response analyzer (FRA).

Cyclic voltammetry (CV) experiments of electrodeposition process were performed in nitric acid (1 M) + lead nitrate (0.25 M) solution, with the aid of Potentiostat/Galvanostat (EG&G 273A) instrument using a three-electrode arrangement of a titanium working electrode, platinum disc auxiliary electrode and Ag/AgCl reference electrode at a scan rate of 20 mV s^{-1}.

Electrochemical properties of lead dioxide samples could be affected by various dissimilar electrolysis parameters and/or alteration of the bath composition during electrolysis. Therefore, a short time electrosynthesis of 240 s of different PT and PTX samples on Pb substrates were performed. These series of Pb electrodes, were subjected to cyclic voltammetry experiments in H_2SO_4 (1 M) deaerated solutions. Cyclic voltammograms (CVs) were recorded at a scan rate of 20 mV s^{-1} in the $PbO_2/PbSO_4$ couple potential region of 0.5–2.15 V. The potential sweeps were initiated at the cell rest potential and scanned towards positive potentials versus Ag/AgCl reference electrode.

2.2. Preparation of electrodes and charge/discharge cycling

Charge/discharge cycle performances of PbO_2 samples were carried out in small laboratory designed batteries using AGM separators (Fig. 1). The composite cathodes were prepared by mixing PbO_2 samples (90% wt.%) and red lead Pb_3O_4 (10 wt.%). The mixture was then pressed at 1 ton cm^{-2} for 1 min on a stainless steel plate to form a cathode disc. Anode gels composed of conventional lead powder with some additives such as $PbSO_4$. Cycling experiments were performed using a computer-controlled battery-testing system. Test cells have been charged at a constant current of 16 mA $g^{-1}PbO_2$ and discharged through a constant resistance of 100 Ω to a cut-off voltage (COV) of 1.75 V.

For the construction of bipolar batteries we have used polyethylene conductive foils, (thickness: 1.5 mm, specific resistance ρ: 2 Ω cm), which are supplied by Zipperling company, Hamburg, Germany. In order to obtain an effective adhesivity, the cathodic face of the polymeric foil is coated with graphite,

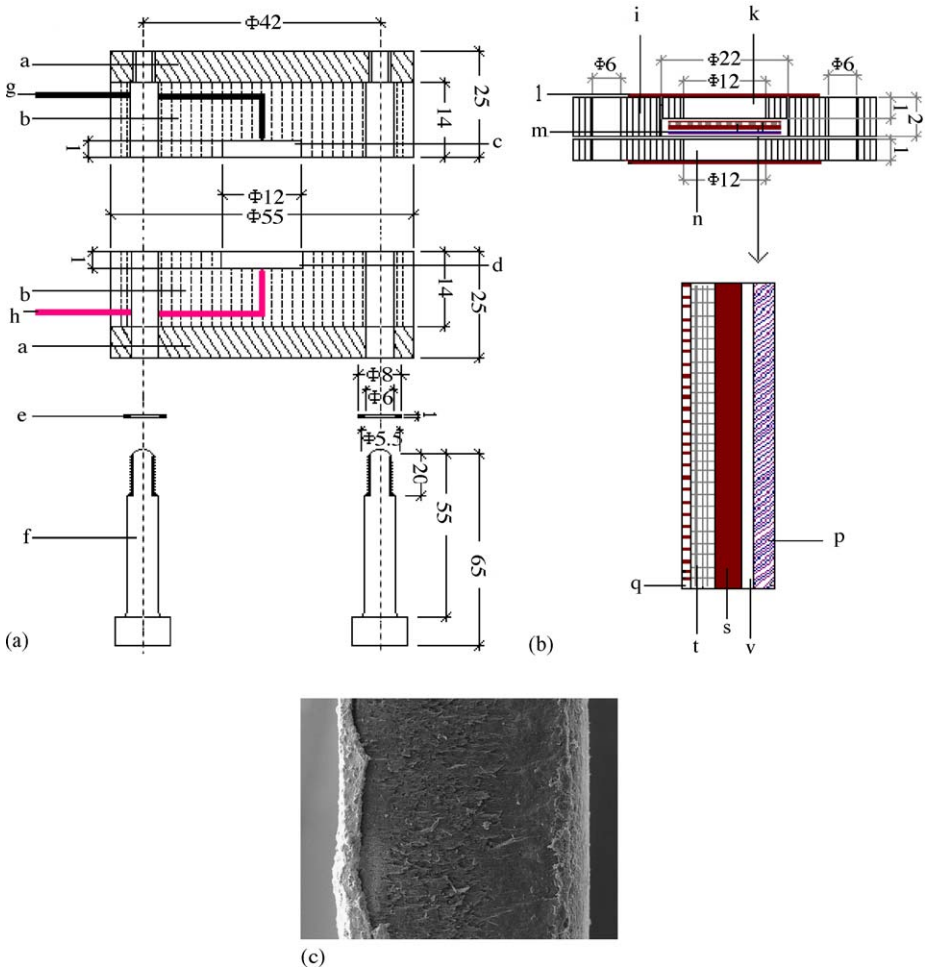

Fig. 1. (a, b) Schematic cross-section views of battery case monopolar and bipolar (with bipolar electrode, left) cell designs. (c) Cross section of a bipolar electrode with a coated layer of Pb on electroless Nickel on the left side and a thin layer of PbO_2 deposited on graphite current collector on the right side of conductive polyethylene substrate. (a) steel disc, (b) polymer container made of PTFE, (polytetrafluroethylene) (c) anode gel container, (d) cathode disc container, (e)gasket (f) screw, (g) and (h) negative and positive terminals (i) PTFE ring, (k) cathode disk, (l) separator, (m) PTFE ring (n) anode gel, (p) lead layer (anode current collector), (q) thin layer of lead dioxide, (s) polyethylene polymer (t) graphite layer (cathode current collector), (v) nickel layer.

using an optimized temperature in the range of 100–110 °C and the pressure of 6 ton/cm^2. A thin layer of PbO_2 was coated on graphite layer. Then, electroless Nickel metallizing of the anodic backside of PE foil was applied before the subsequent electroplating with pure lead. Electroplating of pure lead on electroless Nickel was done in a bath containing lead fluoroborate. A cathodic disc made of PTX100 was then put on the graphite coated cathodic side of the bipolar plate, which has been labelled as Pb-PE-C-PbO_2. Fig. 1b and c show cross-section views of the produced bipolar electrode.

A second type of these electrodes was made with the same polyethylene foil, metallized both sides with electroless nickel. Both sides of the metallized foil was then electrolytically coated with thin layers of Pb and the resulted bipolar electrode has been labelled as Pb-PE-Pb. The composition of cathode disc and anode gel was the same as the first bipolar battery. Both bipolar batteries have been charged at a constant current of 20 mA g^{-1}PbO_2 and discharged through a constant resistance of 1200 Ω to a cut-off voltage (COV) of 3 V. Thin layers of AGM, pressed on porous polystyrene foils, were used as separator for bipolar stack.

3. Results and discussion

3.1. Kinetic aspects of lead dioxide electrodeposition process in the presence and absence of surfactants

PbO_2 active materials are normally prepared by electrochemical methods and the electrocrystallization process is a crucial step determining its electrochemical behavior. The mechanism for the formation of lead dioxide may comprise four stages [5]:

$$H_2O \rightarrow OH_{ads} + H^+ + e \quad (1)$$

$$Pb^{2+} + OH_{ads} \rightarrow Pb(OH)^{2+} \quad (2)$$

$$Pb(OH)^{2+} + H_2O \rightarrow Pb(OH)_2{}^{2+} + H^+ + e \quad (3)$$

$$Pb(OH)_2{}^{2+} \rightarrow PbO_2 + 2H^+ \quad (4)$$

The first stage is an electron transfer process leading to formation of oxygen-containing species of the type OH_{ads} on the electrode surface, (Eq. (1)). Mass transport of lead (II) species from bulk solution to the electrode surface provides the possibility for reaction of OH radicals with Pb^{2+} ions to form some crystal nuclei of the type $Pb(OH)^{2+}$ (Eq. (2)). This product, which is not fixed on the electrode surface is then oxidized with the transfer of a second electron (Eq. (3)) to form tetravalent lead of the type $Pb(OH)_2{}^{2+}$. The latter compound is assumed to be capable of both being accumulated or removed from the electrode surface into the bulk solution [36]. The last stage involves the surface diffusion of lead (IV) species along with oxygen species to become incorporated into the PbO_2 lattice via a chemical mechanism (Eq. (4)). The fastest step in the above mechanism could be attributed to the production of OH radicals [37] and crystal growth takes place in layers of adsorbed intermediate compounds.

Diffusion processes and incorporation of adatoms at lattice sites in the micropores of active mass and in electrolyte are often considered to be crucial steps for crystal growth [38–39]. According to the above mechanism the rate of lead dioxide growth may depend on the amount of intermediate product $Pb(OH)^{2+}$, formed at the electrode surface [40].

It is suggested that in the presence of TX100, production of hydroxyl radicals occur at a slower rate than surface diffusion of deposited species [41]. This assumption based on the fact that formation of hydrophobic layers of surfactants makes the exchanges at the electrode/electrolyte interface more difficult. The decrease of the anodic generation of O_2 may also be attributed to possible interactions of surfactants with the OH radicals, as intermediate for oxygen evolution.

Adsorbed surfactant layer, which may act as a path for Pb^{++} ions, should preferably inhibit very active electrochemical sites (steps, kinks, etc.). In addition, in the presence of surfactant, the surface diffusion of adatoms may be facilitated and hence the creation of excess new nuclei is suppressed. These phenomena give not only a more homogeneous distribution of the current at the electrode/electrolyte interface, but also allows processes to take place slower, i.e., enables the species to find the most suitable positions in the structure [42]. As a result, deposits with densely packed structure, smooth surface and reduced morphological defects (low macropores) could be obtained. This should provide high mechanical strength and adhesion of materials to the substrate.

We observed that adhesion of PTX samples to Ti substrate was higher compared to PT samples. This indicates a decrease in the degree of the residual stress between the PTX/TiO_2 interface. The ease of mechanical separation of all samples appears to have the following trend: PT25 > PTX25 > PT50 > PTX50 > PT75 > PTX7 5 >PTX100. These observations are consistent with the results of cycle performance measurements and EIS. In the absence of surface-active agents, the rate of Eq. (1) is higher and concentration polarization is severe. In this case, nucleation of additional growth centers is a frequent event. Hence, adatoms no longer reach their equilibrium position on the electrode surface and the deposit formed will be less ordered with a higher degree of the roughness, tension and disorder [43].

The temperature influences all diffusion processes like ion diffusion in the electrolyte and surface diffusion of the nuclei [38]. Elevated bath temperatures and higher activation energies, provide much higher much higher surface diffusion of adatoms and/or OH radicals compared to electron transfer. Thus, both surfactants and heat allow relative higher diffusion rate of surface adatoms in relation to the creation of hydroxyl radicals and other oxygen intermediate compounds, which could be capable of being accumulated on the electrode surface.

3.2. Oxygen evolution

Surfactants may strongly adsorb, suppress and/or modify the structure of the hydrous layer so that the electrode surface may be less accessible to water molecules and water discharge is inhibited [44]. Inhibition of the formation of hydrous layer is

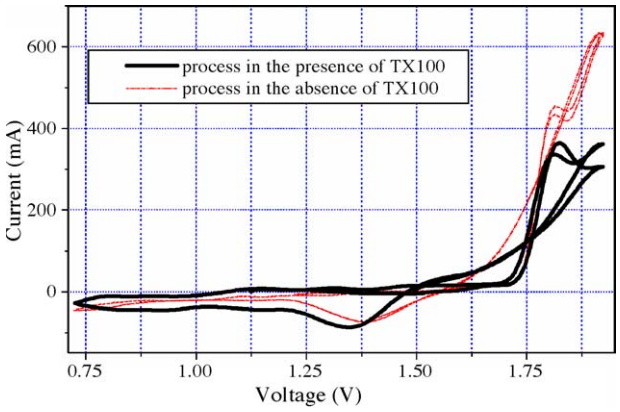

Fig. 2. Cyclic voltammograms of electrochemical process $PbO_2/PbSO_4$ couple potential region carried out in nitric acid + lead nitrate solution in the presence and absence of TX100. CV was performed using a three-electrode arrangement of a titanium working electrode, platinum disc auxiliary electrode and Ag/AgCl reference electrode at a scan rate of 20 mV s^{-1}.

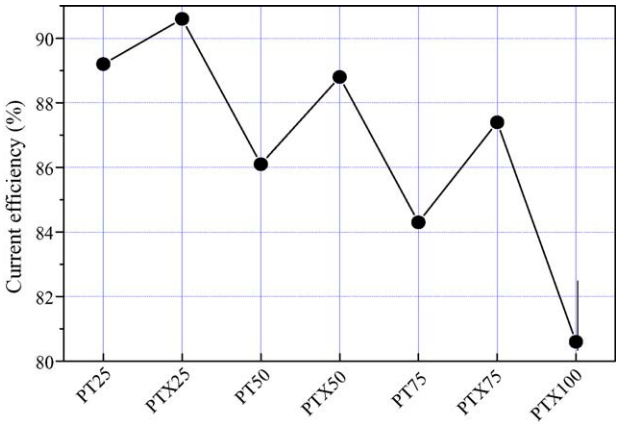

Fig. 3. Current efficiencies for electrodeposition processes of lead dioxide in the presence and absence of TX100. Electrodeposition were performed in standard bath solutions on Ti substrates at current densities $j \leq 10$ mA cm^{-2}.

possible, because the general hydration equilibrium:

$$PbO_2 + H_2O \leftrightarrow PbO(OH)_2 \quad (5)$$

is shifted to the left. Lead dioxide deposition occurs under diffusion control at potentials in the region of oxygen evolution. Evolution of oxygen in acid media is considered to come from discharge of water molecules to form short-lived hydroxyl radicals (OH°), which combine subsequently to produce oxygen molecules:

$$2OH^\circ \rightarrow O_2 + 2H^+ + 2e^- \quad (6)$$

Hydroxyl radicals are bound to active centers located in the hydrous layer [45], which could be considered as the immediate source of oxygen atoms. In the process of PbO_2 electrodeposition, some of the oxygen-containing species directly transfer to form oxygen and evolve away from the solution [43]. The formed oxygen may cause cracks in the oxide structure and this in turn will result in a more porous and uneven surface oxide structure. The suppression of a number of active sites by TX100 decreases the density of reaction intermediates, and the Oxygen evolution potential will rise (Fig. 2). Oxygen evolution contributes significantly to the total current thus decreasing the current efficiency of lead dioxide formation.

Results have shown that current efficiencies for the formation of PTX samples were higher due to inhibition of oxygen evolution through adsorbed layer of surfactant molecules (Fig. 3). In this regard, the effect of surfactant could be interpreted as decreasing the amount of labile oxygen species, which could be removed form the electrode surface into the electrolyte solution. It must be noted that bath temperature could also affect the hydration state of the surface and hence the oxygen evolution potential. However, for determining of the effect of different bath temperatures, on oxygen evolution potential during synthesis of PT and PTX samples, voltammetric experiments must be carried out at different bath temperatures. Anyway, results of current efficiencies for the production of PT or PTX series have shown that an increase in bath temperature results in a decrease of current efficiencies in each PT or PTX series. It might be suggested that with an increase in bath temperature, the accumulation of the labile oxygen species decrease (similar effect of heat to TX100). These species like Pb(III) or Pb(IV) compounds, may be removed form the electrode surface into the electrolyte solution.

3.3. Electrochemical charge/discharge performances

Discharge capacities of all test cells, each containing the same amount of PT and PTX samples, are shown in Fig. 4. Cell parameters and test procedures were held constant for all samples. Results show, that cumulative discharge capacities of PTX samples are higher (Fig. 5) and the extent of voltage dips is lower, compared to those of corresponding PT samples.

The voltage dip followed by a recovery, commonly known as "coup de fouet" [46]. This is associated with a discharge process occurring at the Pb/PbO_2 interface [47]. Fig. 4d show that the extent of voltage dip is lowest in PTX100. This indicates that the selected rout for modifying samples, through both increasing bath temperature and the presence of surfactants, has a positive effect on lowering the passivation phenomena at the Pb/PbO_2 interface.

It has been demonstrated that the discharge capacity of lead dioxide was not proportional to its BET surface area [48]. It exists obviously other important factors, which could influence the discharge performance of different modifications of PbO_2.

One of the major factors influencing the discharge capacity of lead-acid batteries was shown to be connected to the PAM type and the related interparticle contact, which is more important than porosity [49]. The less porous the active material, the better is the chance for a good interparticle contact and higher discharge capacity. It has been shown that despite the reduced pore volume the capacity of electrodes with higher PAM density is higher than that of their counterpart with lower PAM density [50]. This indicates that the electronic conductivity as well as ion diffusion in the porous lead dioxide system plays important role during charge and discharge. Many results showed that a more porous electrode received a capacity loss due to increased IR-drop, which in turn may caused by a decreased interparti-

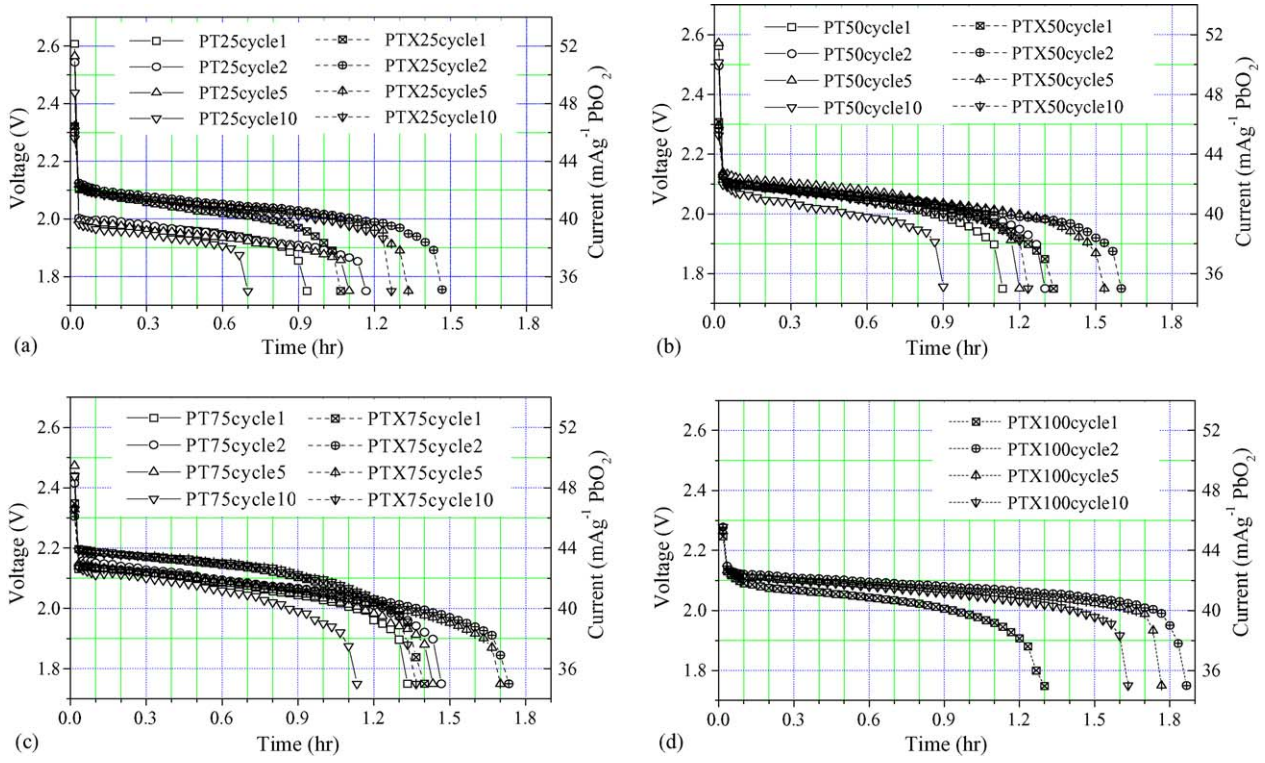

Fig. 4. Discharge curves of test cells containing different lead dioxide samples. PbO_2 samples are electrodeposited in standard bath solutions on Ti substrate at current densities $I \leq 10\,mA\,cm^{-2}$. Cells are discharged at a constant resistance of $R = 100\,\Omega$ to a cut-off voltage of 1.75 V. Charging is done at constant limited current of $16\,mA/g^{-1}$ PbO_2.

cle contact. Thus, the lower capacities of PT samples could be attributed to a poor mechanical strength, lower conductivity due to a lower crystallinity and other related phenomena like lower ion diffusion process.

Another factor influencing the discharge capacity is the surface morphology as well as the size of the PbO_2 crystals. If the size of crystals became smaller, the discharge capacity decreased, because the electrode may be passivated with a smaller amount of $PbSO_4$ [51]. Formation of morphological defects like cracks and macropores on PbO_2 surface could also contribute to a decrease in discharge capacity of test cells. Since the electrochemical path involves the formation of high crystalline lead sulphate as an intermediate stage, some of the sulphate will be trapped in the defect zones of lead dioxide surface by adsorption [52]. This type of lead sulfate cannot, or only partially, be reconverted back to an electrochemically active form. This phenomenon weakens the bonds between the PbO_2 crystals and the conductivity is reduced. The voluminous $PbSO_4$ causes breaking and weakening of the mechanical integrity of the plate and loss of capacity [53]. In addition, deposition of lead sulfate does not occur uniformly throughout the bulk of active material, so variation of conductivity and current density occur, as current flow will concentrate in areas of good electrical contact adjacent to cracked region. Thus, non-uniform current distribution over the electrode surface causes a change in rates of heat generation and cracks formations. However, other phenomenon like oxygen evolution at the positive plates due to self-discharge may then represent an important part of total water loss and decrease of capacity, especially in the case of PT samples.

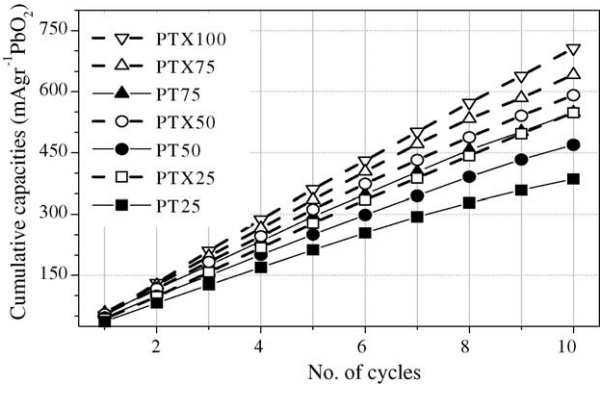

Fig. 5. Cumulative capacities of laboratory test cells extracted from Fig. 4.

The higher discharge capacity of PTX samples could be explained via Solid-state reaction model [54]. This model considers solid-state discharge reactions, with the passage of ionic current under high fields through the PbO passivating film on PbO_2 surface (Eq. (7)). However, the reduction process proceeds also in the interior of the aggregates. It is considered that H^+ ions penetrate in the aggregates interior, and H_2O and Pb^{2+} ions pass in the opposite direction, whereas SO_4^{2-} ions cannot penetrate into the interior of the aggregates. With progressively formation of PbO passivation layer, the field through the formed PbO layer slowly disappears. This makes the entrance of SO_4^{2-} at the initial pore surface easy and the chemical transformation of the PbO to disrupted $PbSO_4$ is now possible (Eq. (8)). The

disrupted microcrystals recrystallize to larger particles [55].

$$PbO_2(\text{solid surface}) + 2H^+(\text{solution}) \rightarrow PbO(\text{film}) + H_2O(\text{solution}) \quad (7)$$

$$PbO(\text{film}) + yH_2SO_4(\text{solution}) \rightarrow xPbO(\text{adherent}) + yPbSO_4(\text{disrupted film}) + yH_2O \quad (8)$$

PTX samples are characterized with a lower amount of amorphous phase and enhanced diffusivity. The higher crystallinity and mechanical strength, the more is the association of positive active material and electrical conductivity. Probably, because of higher field strength and higher proton diffusivity within the solid phase, the reaction 7 could proceed relatively to a higher extent before the entrance of SO_4^{2-} particles takes place at the initial pore surface. Consequently, discharge capacities of these modified samples increased compared to corresponding unmodified samples.

3.4. Possible relation between PAM type, interface corrosion and capacity loss

Both PAM type and grid alloy composition affect the corrosion layer properties [56]. One of the major factors, which may be connected to the capacity loss of PT samples, is the corrosion at the PbO_2/Pb interface. In these corrosion processes, the amount and movement of surface-adsorbed water across PbO_2 is an important factor [1]. Water, may react at the inter-crystalline surface of PbO_2 particles to form surface OH groups. These groups, which may be considered as the result of inter-crystalline surface reaction of water and PbO_2 particles, may provide sites for relatively mobile surface protons. This would allow the ionic current flow in electrochemical corrosion process. Surface-adsorbed H_2O molecules may move from the electrolyte/PbO_2 interface to the PbO_2/Pb interface to react with Pb^{4+} ions, forming PbO_2. This type of PbO_2 precipitates, in the absence of sulfuric acid, in the form of the α-modification on Pb/PbO_2 interface.

The corrosion processes, which occur under open-circuit conditions, would also require the transfer of water molecules and the formation of hydration layer. This phenomenon may also stay in connection with the PAM type and its ability to adsorb and transport the water molecules. The *anodic* oxidation of lead at the Pb/PbO_2 interface is now being driven by a simultaneous *cathodic* reduction of PbO_2 at the PbO_2/electrolyte interface. The overall reaction is then [1]:

$$2\beta\text{-}PbO_2 + 2H_2SO_4 + Pb \rightarrow \alpha\text{-}PbO_2 + 2PbSO_4 + 2H_2O \quad (9)$$

The formation of lead sulfate in the corrosion layer will lead to mechanical stress, causing the formation of crevices, or cracks, which in turn may accelerate water transfer and thus increase the corrosion rate. It could be suggested that the amount and transport of adsorbed water molecules across active material may be higher in the case of PT samples and thus the extent of corrosion process is higher compared to modified samples.

Another important factor, which is related to the formation of corrosion layer, is the action of oxygen gas. O_2 is obviously generated easier on unmodified PbO_2 samples (Fig. 8). During operation and overcharging of a battery, oxygen gas reacts with the positive grid forming a lead monoxide corrosion layer. This subsequently reacts electrochemically to form lead dioxide resulting in the formation of a corrosion layer containing both, lead monoxide and lead dioxide [57]. The change in molar volume that occurs when Pb is oxidized to PbO_2 is >38% [56]. A consequence of this is the generation of internal stresses, which cause cracks and reduces the mechanical strength, conductivity and hence the cell capacity.

Since the contribution of metallic lead in interface corrosion is very high, we decide to design a light bipolar battery based on conductive plastics with carbon current collector. For the construction of lightweight bipolar batteries, we have investigated the possible use of carbon filled conductive polyethylene substrate [34]. In this regard, two types of bipolar batteries were constructed as described in Section 2.1.

The polarization diagrams and cumulative capacities of both type of bipolar batteries show a rather similar performance as could be seen in Figs. 6 and 7, respectively. This result indicates that usage of carbon collector substrate instead of lead on polyethylene substrate has obviously no negative effects on charge/discharge cycle performances in our experimental conditions and the weight reduction of such batteries is possible. Results of bipolar batteries based on conductive polyethylene foil are in initial stages and more detailed experiments must be conducted for further enhancement.

3.5. Cyclic Voltammetry of PbO_2 samples deposited on Pb

Fig. 8 shows that a single reduction peak of PbO_2 observed as a well-defined peak in the range of +1.1 to +1.3 V. During reduction, β-PbO_2 from the outer sub layer transforms to a passivation layer of lead sulphate at the electrode surface. Reduction peaks are broad because the process involves two solid compounds: lead dioxide and lead sulphate, and needs the diffusion of protons and sulphuric acid into the active mass [58].

Reduction peaks of PTX samples are more broad and larger compared to those of PT samples. However in latter samples the reduction potentials are shifted to more positive potentials. This could be explained through lower mechanical strength and/or higher morphological defects, which allows an easy diffusion of sulfuric acid into the sample. It could be suggested that the surface of PT samples, especially PT25 is more active, specially in regions with more lattice distortion or lattice incompletion. The more positive reduction potential in PT samples may be connected to a lower conductivity, lower field strength and hence easier access of SO_4^{2-} ions to the formed surface PbO layer. The following strong current suppression seems to be due to decreased diffusivity of the protons within the PbO_2 crystal lattice (higher warburg impedance) and/or higher passivity of electrode through the formed $PbSO_4$.

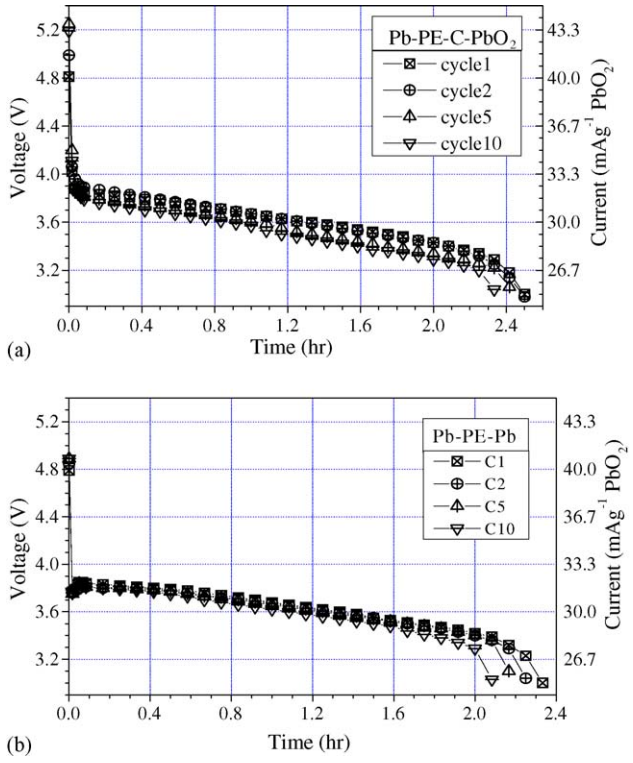

Fig. 6. Polarization diagrams of bipolar batteries with (a) Pb-PE-C-PbO_2 bipolar electrode, made of Polyethylene. The anodic side of this electrode consists of a Pb layer coated on electroless Nickel. Pb layer was deposited from a bath containing lead fluoroborate with a current density of 2 mA cm^{-2}. The cathode side is a thin layer of graphite coated on PE substrate. (b) Pb-PE-Pb bipolar electrode. This is bipolar electrode with PE substrate, which are at first both sides are metallized with electroless Nickel and then a thin layer of Pb is coated on electroless Nickel. Batteries are charged at 20 $mAg^{-1}PbO_2$ and continuously discharged at constant resistance of 1200 Ω to a cut-off voltage of 3 V.

During anodic-going sweeps the PbO layer is oxidized to non-stoichiometric oxide PbO_x, (where $1<x<2$). When x reaches a critical value, α-PbO_2 nucleation starts at the PbO_x membrane interface [59]. On the anodic sweep, two peaks are observed corresponding to α and β-PbO_2 formation. The oxidation peak area corresponding to the formation of β-PbO_2 is increased for PTX samples and the corresponding potential shifted to more positive potentials. The main anodic electrode reaction is accompanied

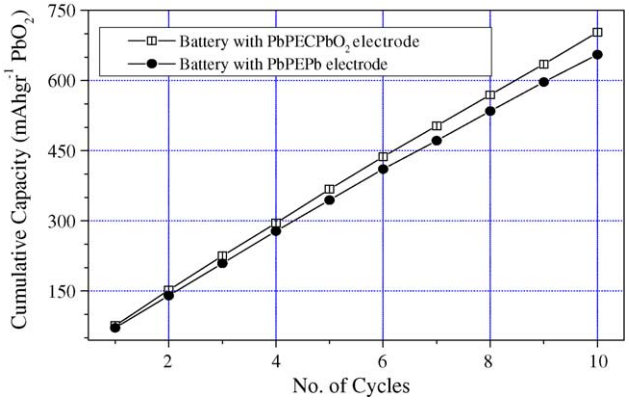

Fig. 7. cumulative capacities of test bipolar batteries, extracted from Fig. 6.

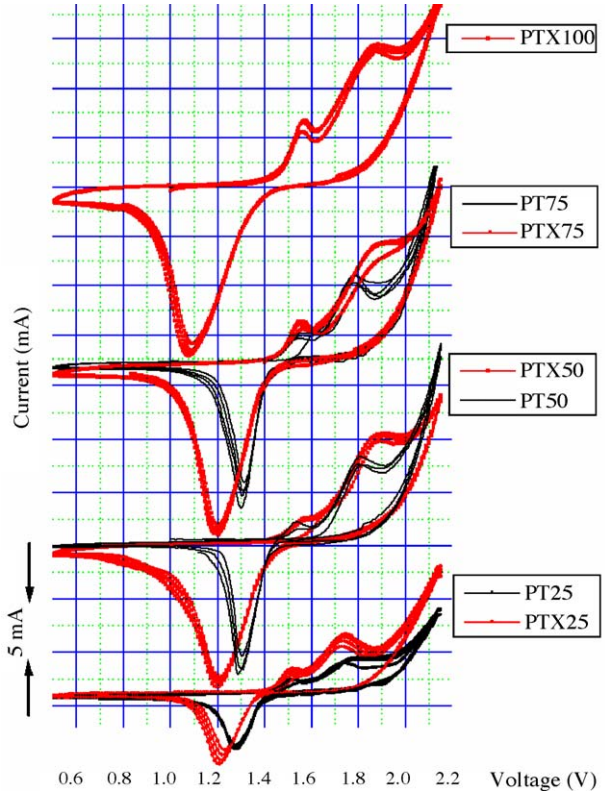

Fig. 8. Cyclic voltammograms of PbO_2 samples carried out in H_2SO_4 solutions (1 M). Lead dioxides were electrodeposited in standard bath on lead foils for 240 s. CVs are recorded at a scan rate of 20 mV s^{-1} with Ag/AgCl reference electrode and Pt auxiliary electrode.

with O_2 evolution. The peak at potentials higher than 1.9 V features a current growth that corresponds to the oxygen evolution. The shift of this peak to more positive potentials in PTX samples indicates a retardation of oxygen evolution reaction. Oxygen evolution accompanied by a number of secondary reactions like corrosion of Pb current collector and cracks formation. As could be seen from voltammograms, the oxygen evolution potential is lowest in samples PT25 and PTX25 compared to samples prepared at higher bath temperatures. This indicates the strong influence of synthesis temperature on physico-chemical characteristics and hence oxygen evolution reaction. Results indicate that increasing bath temperature form 50 to 75 °C has no significant effect on oxygen evolution potential of the obtained materials PT50 and PT50. However, in comparison to latter samples, the overpotential for oxygen evolution is still increased to a considerable amount for modified samples PTX50 and PTX75.

3.6. SEM

Proper functioning of batteries depends not only on the structure, but also on the morphology of the active materials [60]. Fig. 9 present the SEM micrograph of different PbO_2 samples with a magnitude of 3000, when Ti substrate is used. There is a notable difference between the microstructural features of modified samples with a relatively more regular morphology and those of unmodified samples with a higher degree of surface roughness, macroporosity/cracks. For example, both sam-

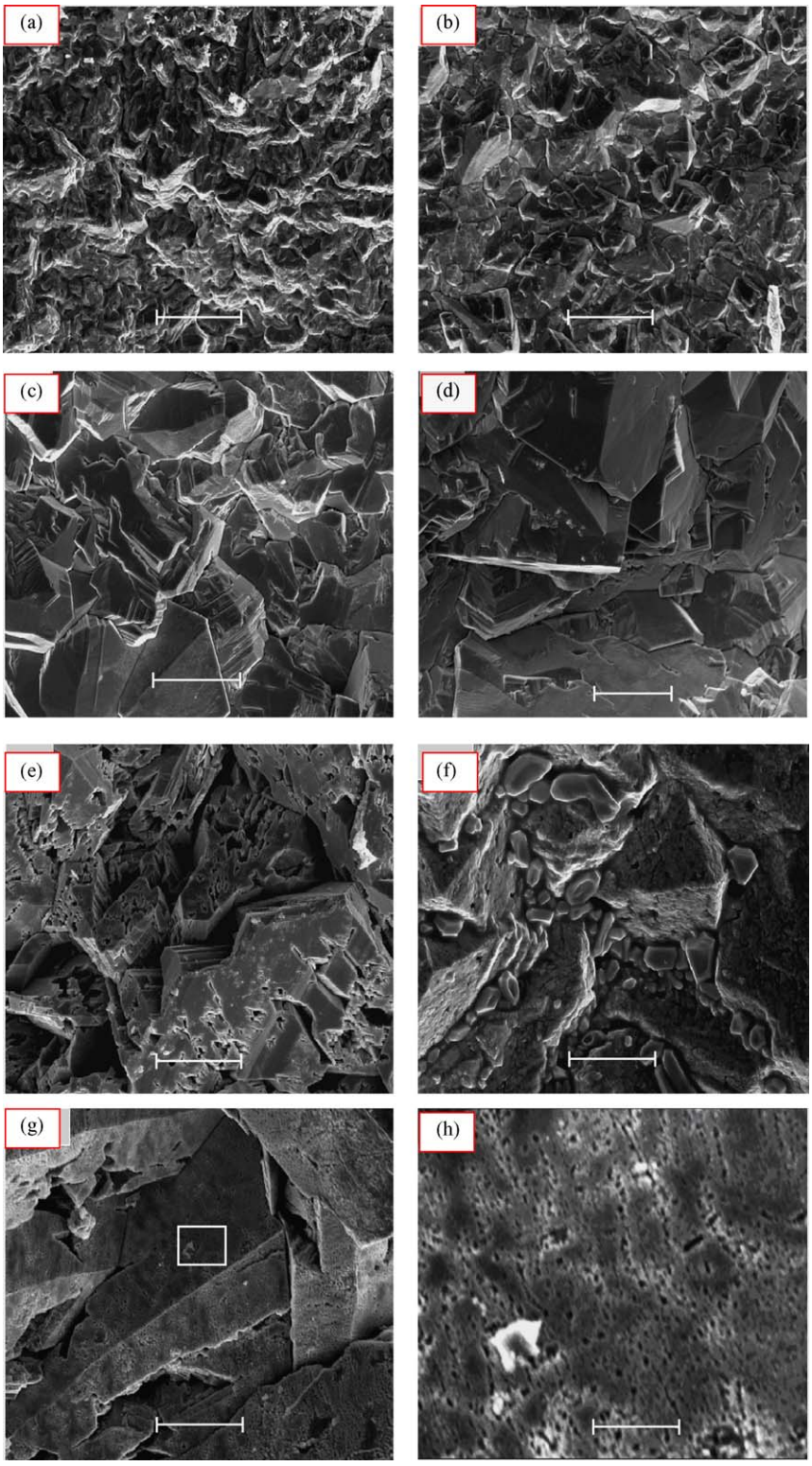

Fig. 9. Scanning electron micrographs of different PbO_2 films. Samples are coated with approximately 5 nm of gold. The magnification indicated by a bar with a dimension of 20 μm. (a) PT25, (b) PTX25, (c) PT50, (d) PTX50, (e) PT75, (f) PTX75, (g) PTX100, (h) higher magnification of the rectangle marked in micrograph (g) with a bar dimension of ca. 2.5 μm.

ples produced at 25 °C have a weak structural strength and/or density because of lower bath temperature during electrosynthesis. However, in PTX25 the crystalline structure is essentially enhanced with edges and apexes are more pronounced, whereas these features could not be recognized in PT25 (Fig. 9a and b).

Defects are normally could be observed within the bulk of active material in the form of cracks and pores due to

Table 1
Parameters from X-ray diffractogram measurements

PbO_2 Samples	25.4°2θ		28.5°2θ	32.05°2θ	
	Wide	Height	Height	Wide	Height
PT25	0.402	1581	191	0.442	2202
PTX25	0.326	2714	223	0.318	3119
PT50	0.262	2560	69	0.268	2728
PTX50	0.248	2721	61	0.254	2740
PT75	0.229	4086	85	0.235	4358
PTX75	0.219	4707	79	0.222	4518
PTX100	0.188	6547	147	0.199	5715

stress within the active material (compare PT75, PTX75). These defects could have two mainly effects. On one side, they act to reduce the effective electrical conductivity of the layer, as electron cannot flow across cracks. On the other side, they increase diffusion rates of gases, such as oxygen escaping through the different parts of PAM by provision of an easy pathway.

Optimized electrocrystallization of PbO_2 is obtained in the presence of surfactant at a bath temperature of 100 °C (the corresponding PbO_2 sample labeled as PTX100), as can be seen in the details of Fig. 9g. The notable difference between PTX100 and other samples is that the lead dioxide pyramidal structures are pitted with a high number of micropores (Fig. 9h as a higher magnification of Fig. 9g). The diameters of these pores are in the range of 100 nm to a few hundred nm. These features suggest higher penetration of electrolyte into micropores and ultimately proton mobility within the oxide lattice and increased electrical conductivity and a lower charge transfer resistance as confirmed by EIS.

3.7. XRD

The increase in bath temperature is accompanied with a higher degree of crystallinity of the obtained lead dioxide samples. However, the degree of crystallinity is higher for samples produced in presence of surfactants. X-ray diffraction patterns indicate a marked decrease in peak width of the diffraction lines and an increase in peaks intensity in PTX samples compared to corresponding PT samples (Table 1). It could be observed that the extent of lattice spacing, which is highest in the case of PT25, is reduced in PTX25. The broadening of diffraction lines is the result of two related phenomena: a reduction of crystallites and an increase in the range of microscopic stresses [61].

Another difference between the PT and PTX samples is the level of background. As could be seen from diffractogramms, background of the PT25 is largest indicating a higher amount of amorphous material [52]. The density of the diffraction peaks increases and the peak width decreases in the order TX100 > PTX75 > PT75 > PTX50 > PT50 > PTX25 > PT25. This result is in accordance with the observation of mechanical removing of the samples form Ti substrates. In other words, the more crystalline is the sample, the harder is its adherence to Ti substrate (Fig. 10).

The results show that the amount of crystallographic modification α-PbO_2 are depend on preparation procedures. The

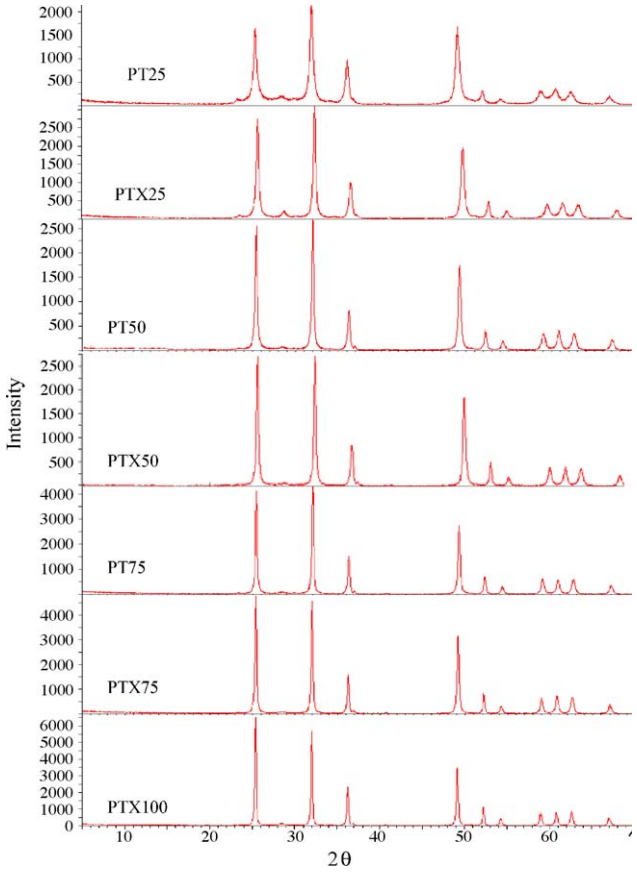

Fig. 10. X-ray diffractograms of PbO_2 Powders.

percentage of the α form, W_α, is calculated by Munichandraiah using the following relation:

$$W_\alpha = \frac{2J_\alpha}{K(J\beta_1 + J\beta_1)} \quad (10)$$

where K is a constant, which could be also calculated using a known mixture of α and β-PbO_2 [62]. The β-PbO_2 form may be identified from its most intense lines (110, at 25.4°2θ) and (101, at 32.05°2θ), and the α form from its (111, at 28.5°2θ) line. The relative intensities of these lines are denoted as $J\beta_1$, $J\beta_2$ and J_α, respectively. Results indicate that at a low bath temperature of 25 °C the relative amount of W_α is higher compared to higher bath temperatures. However, in the presence of TX100, i.e., in PTX25, the amount of the α form is reduced. At bath temperature 50 and 75 °C, the effect of TX100 on W_α, have been assumed as negligible and a correlation between the amount of α-PbO_2 and the electrochemical performance cannot be realized.

3.8. Electrochemical impedance investigation

Fig. 11 present the Nyquist diagrams for PT and PTX samples. The simulation of experimental and calculated parameters was evaluated using Z-view software. Fig. 12 represents the equivalent circuit (EC) for the open boundary finite length diffusion model. The elements used in this EC are constant phase element (CPE), solution resistance (R_s), charge transfer resistance (R_c) and Warburg resistance (Z_w). A generalized CPE

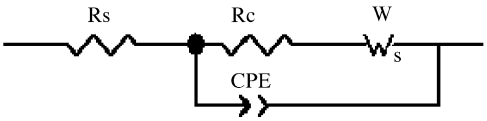

Fig. 11. Suggested equivalent circuit.

describes the non-ideal behavior of the capacitance. The fitted data follows in a satisfactory fashion the experimentally obtained impedance responses, thus confirming the validity of the simulation. The impedance of CPE is given by [62]:

$$Z_{\mathrm{CPE}} = [Q\,(j\omega)^n]^{-1} \tag{11}$$

which models the diffusion impedance when the diffusion layer has finite dimensions [63]. j is the imaginary number, Q is the frequency-independent real constant, $\omega = 2\pi f$ is the angular frequency (rad/s), f is the frequency of the applied signal and n is the CPE exponent. For a diffusion-controlled process the impedance is given by:

$$Z_{\mathrm{w}} = \frac{[\tanh\ B(j\omega)^{1/2}]}{Y_0(j\omega)^{1/2}} \tag{12}$$

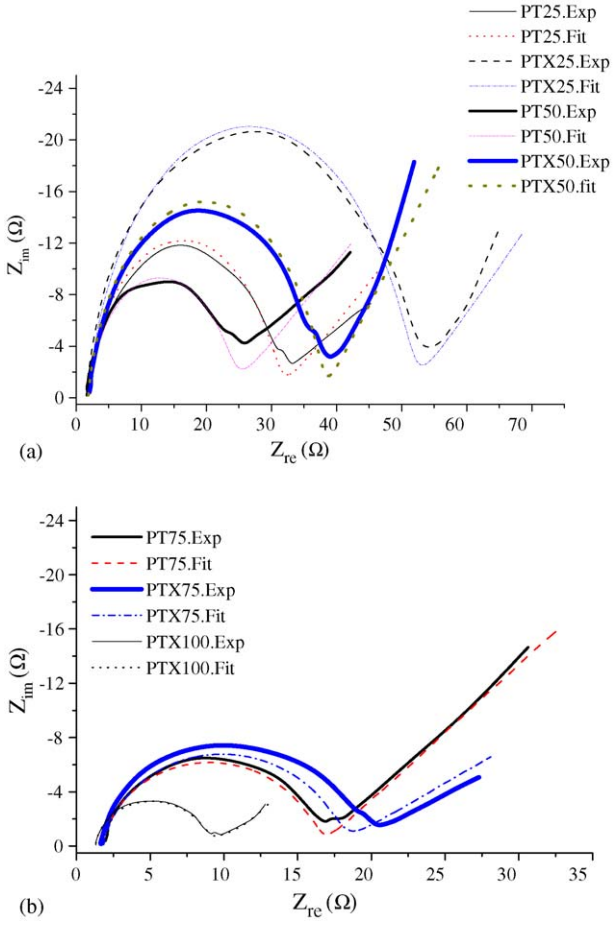

Fig. 12. Impedance plots for PbO_2 films electrodeposited on Ti from standard bath for 28 min. EIS was performed in H_2SO_4 (1 M), with Ag/AgCl reference electrode and Pt auxiliary electrode (Pt) in a frequency range of 100 kHz to 100 mHz.

Table 2
Calculated equivalent parameters

Sample	R_s (Ω)	R_c (Ω)	Z_w (Ω)	n	σ (Ω cm^2 s$^{-1/2}$)	|B| (s$^{1/2}$)
PT25	1.83	27	6.5	0.9	8.7942	0.2345
PT50	1.83	20	5	0.9	27.70	0.1726
PT75	1.83	15	3.5	0.9	10.26	0.2132
PTX25	1.83	48	3.75	0.9	9.2435	0.4244
PTX50	1.83	35	3.2	0.9	6.2174	0.4141
PTX75	1.83	14	2.8	0.9	5.1747	0.2601
PTX100	1.77	7	0.8	0.9	5.5797	0.1269

Where $B = \iota/(D)^{1/2}$, D is the diffusion coefficient, ι is the diffusion layer thickness, $Y_0 = (\sigma(2)^{1/2})^{-1}$ and σ is the warburg coefficient. The diffusion layer thickness ι could be calculated using the B values obtained from Table 2, if the diffusion coefficient of protons in PbO_2 samples is known. Table 2 shows the fit parameters for all PT and PTX samples. It is clear from Table 1 that in PTX samples values of R_c are lower indicating enhanced interfacial phenomena compared to PT samples. The n values listed in Table 1 were close to 1, which indicate the behavior of an ideal capacitor. The theoretical value of σ can be calculated using the following equation [64]:

$$\sigma = \left(\frac{RT}{(2)^{1/2} n_2 F_2}\right)(C(D)^{1/2})^{-1} \tag{13}$$

Where R is the real gas constant (JK^{-1} mol^{-1}), T is the absolute temperature (K), F is the Faraday constant, C is the concentration of protons, n is the number of electrons and d is the diffusion coefficient of protons. For the known values of Warburg coefficient and diffusions coefficient of protons, the concentration of protons (c) in the sample can be calculated and compared with real concentrations.

We believe that the most relevant difference remains between the values of Warburg impedance Z_w, which is due to microporosity of PbO_2 and proton diffusivity within interior of the solid structure. Results indicate that the values of Z_w is lower and hence the diffusion of ions is enhanced in PTX samples compared with corresponding PT samples. The lower Z_w values prove that PTX samples have a shorter diffusion path length compared to corresponding PT samples. A shorter diffusion path length is accompanied with higher B values as could be seen in Table 2.

3.9. Thermal degradation of PbO_2 samples and their relationship to capacity

Hydrogen atoms can be incorporated into the PbO_2 crystal structure by a variety of mechanisms: (i) coupled substitution of $(OH)^-$ for O^{2-}, and Pb^{2+} for Pb^{4+}; (ii) direct substitution of $4H^+$ for Pb^{4+}; (iii) as interstitial protons, with mobile electrons [65]. These have been suggested as explanations to the structural disorder of $PbO_{2-\delta}.mH_2O$ [42]. δ denotes an oxygen deficiency with a value in the range of 0.04–0.06 and m the structural water content. According to the hydrogen-loss model [66–68], the electrochemical activity is determined by hydrogen that has been incorporated in the PbO_2 crystal lattice. It is

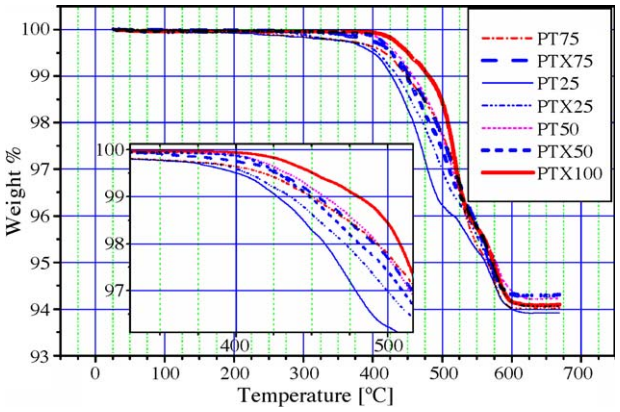

Fig. 13. TGA curves of PbO_2 samples between RT and 700 °C at 10 °C min^{-1}.

argued that PAM contains two types of hydrogen: the first type of hydrogen species is associated with mobile and/or isolated, adsorbed hydroxyl groups and/or water molecules that can be removed by outgassing [69]. It is most likely that the second type of hydrogen species corresponds to more strongly bound water molecules and/or closely spaced hydroxyl groups trapped on internal crystal surfaces. This type is associated with particle cracking prior to structural decomposition of the PbO_2 to PbO, at 350–550 °C [65]. The relative masses and relative abundance of water evolved during these two stages vary and are dependent on preparation procedures.

A correlation of type and relative abundance of water or hydrogen species with battery performance was found in this work. According to Fig. 13, the amount of physisorbed water molecules, or hydrogen species, which may be released in low temperature region of ≤200 °C are negligible. However, removal temperatures of the more strongly bound hydrogen species play obviously important roles in the electrochemical charge/discharge process of PbO_2. While the weight reduction of PTX100 is just 1% up to a temperature of 480 °C, nearly 4% weight reduction could be observed for PT25 in the same temperature region. It could be suggested that the degree of crystallinity, mechanical strength and water removal temperature is connected to electrochemical cycle performances.

4. Conclusion

The type and physicochemical properties of PAM appear to be one of the more influential factors affecting the electrochemical behavior or lead acid batteries. Interesting evidence showed that physico-chemical properties of the obtained PbO_2 samples could be readily controlled by electrochemical technique conditioned by the nonionic surfactant Triton X-100. Electrodeposition of PbO_2 from nitric acid solutions, in the presence of surfactants in the bath, results in a higher crystallinity, enhanced morphology and better coherence between individual PbO_2 particles.

It could be concluded that Triton X-100 causes a decrease in the rate of water discharge based solely on measurement of current efficiencies. Complementary cyclic voltammetry measurements reveal that the adsorbed Triton X-100 molecules lead to a higher anodic overpotential for oxygen evolution. These experiments show also that oxygen evolution shift to more positive potentials in the case of modified samples.

The reason for the improvement of the charge/discharge cycle performances seems to be the stabilization of the positive active material preventing swelling of the active mass and thus reducing the capacity loss. These improvements could also be obtained with an increase in the bath temperature. The lower the bath temperatures, the smaller are the crystallites and the higher is the amount of an amorphous phase. However, in all bath temperatures, the degree of crystallinity and the electrochemical activity is higher, if Triton X-100 is present in the bath.

We believe that the most relevant factors influencing the electrochemical behavior of lead dioxide, are the enhanced conductivity and facilitated diffusivity of more strongly bound hydrogen species into and out of the solid structure. Preliminary electrochemical tests of bipolar batteries show that conductive carbon filled polyethylene with graphite current collectors could be successfully used for construction of lightweight batteries. Results are in initial stages and more detailed experiments must be conducted for further enhancement.

References

[1] P. Ruetschi, J. Power Sources 127 (2004) 33.
[2] E. Meissner, H. Rabenstein, J. Power Sources 40 (1992) 157.
[3] M. Dimitrov, D. Pavlov, J. Power Sources 93 (2001) 234.
[4] D.B. Edwards, S. Zhang, J. Power Sources 135 (2004) 297.
[5] A.B. Velichenko, R. Amadelli, E.A. Baranova, D.V. Girenko, F.I. Danilov, J. Electroanal. Chem. 527 (2002) 56.
[6] R. Amadelli, L. Armelao, E. Tondello, S. Daolio, M. Fabrizio, C. Pagura, A. Velichenko, Appl. Surf. Sci. 142 (1999) 200.
[7] M. Perrin, H. Döring, K. Ihmels, A. Weiss, E. Vogel, R. Wagner, J. Power Sources 95 (2001) 85.
[8] P.T. Moseley, D.A.J. Rand, J. Power Sources 133 (2004) 104.
[9] D.A.J. Rand, J. Power Sources 64 (1997) 157.
[10] C. Bemelmans, T. O'Keefe, E. Cole, Bull. Electrochem. 12 (1996) 591.
[11] T.C. Wen, M.G. Wei, K.L. Lin, J. Electrochem. Soc. 137 (1990) 2700.
[12] Y. Sato, K. Hishimoto, K. Togashi, H. Yanagawa, K. Kobayakawa, J. Power Sources 39 (1992) 43.
[13] U. Hullmeine, E. Voss, A. Winsel, J. Power Sources 30 (1990) 99.
[14] S. Sternberg, V. Branzol, L. Apateanu, J. Power Sources 30 (1990) 177.
[15] E. Voss, U. Hullmeine, A. Winsel, J. Power Sources 30 (1990) 33.
[16] E. Hasik, M. Paszkiewicz, J. Power Sources 30 (1990) 107.
[17] H. Sanchez, Y. Meas, I. Gonzalez, M.A. Quiroz, J. Power Sources 32 (1990) 43.
[18] J.F. Rusling, Acc. Chem. Res. 24 (1991) 75.
[19] J.F. Rusling, Micropor. Mater. 3 (1994) 1.
[20] J.F. Rusling, Colloids Surf. 81 (1997) 123.
[21] G.S. Attard, P.N. Bartlett, N.R.B. Coleman, J.M. Elliott, J.R. Owen, J.H. Wang, Science 278 (1997) 838.
[22] I. Nandhakumar, J.M. Elliot, G.S. Attard, Chem. Mater. 13 (2001) 3840.
[23] T. Gabriel, I.S. Nandhakumar, G.S. Attard, Electrochem. Commun. 4 (2002) 610.
[24] M. Ghaemi, L. Khosravi-Fard, J. Neshati, J. Power Sources 141 (2005) 340.
[25] M. Ghaemi, Z. Biglari, L. Binder, J. Power Sources 102 (2001) 29.
[26] E. Gyenge, J. Jung, B. Mahato, J. Power Sources 113 (2003) 388.
[27] M. Cruz, L. Hernán, J. Morales, L. Sánchez, J. Power Sources 108 (2002) 35.
[28] K. Das, A. Mondal, J. Power Sources 89 (2000) 112.
[29] M. Coux, X. Muneret, P. Lenain, J.L. Wojkiewicz, J. Renard, J. Power Sources 78 (1999) 115.
[30] P. Lailler, J.-F. Sarrau, C. Sarrazin, J. Power Sources 95 (2001) 58.

[31] A.D. Turner, P.T. Moseley, J.L. Hutchinson, in: K.R. Bullock, D. Pavlov (Eds.), Proceedings, vol. 84–14, The Electrochemical Society, NJ, 1984, pp. 267–273.
[32] D. Pavlov, J. Power Sources 53 (1995) 9.
[33] Yu. Kamenev, A. Kiselevich, E. Ostapenko, J. Power Sources 110 (2002) 133.
[34] M. Ghaemi, R. Amrollahi, F. Ataherian, M.Z. Kassaee, J. Power Sources 117 (2003) 233.
[35] M. Ghaemi, R.K. Ghavami, L. Khosravi-Fard, M.Z. Kassaee, J. Power Sources 125 (2004) 256.
[36] A.B. Velichenko, E.A. Baranova, D.V. Girenko, R. Amadelli, S.V. Kovalev, F.I. Danilov, Russ. J. Electrochem. 39 (2003) 615.
[37] M. Fleischmann, J.R. Mansfield, H.R. Thirsk, H.G.E. Wilson, L. Wynne-Jones, Electrochim. Acta 12 (1967) 967.
[38] H. Natter, R. Hempelmann, Electrochim. Acta 49 (2003) 51.
[39] J.A.M. Sondag-Huethorst, L.G.J. Fokkink, Langmuir 11 (1995) 4823.
[40] A.B. Velichenko, D.V. Girenko, S.V. Kovalyov, A.N. Gnatenko, R. Amadelli, F.I. Danilov, J. Electroanal. Chem. 454 (1998) 203.
[41] Y. Matsumoto, M. Noguchi, T. Matsunaga, J. Phys. Chem. B 103 (1999) 7190.
[42] I. Petersson, E. Ahlberg, B. Berghult, J. Power Sources 76 (1998) 98.
[43] P.K. Shen, X.L. Wei, Electrochim. Acta 48 (2003) 1743.
[44] G. Juhel, B. Beden, C. Lamy, J.M. Leger, R. Vignaud, Electrochim. Acta 35 (2) (1990) 479.
[45] R. Amadelli, A. Maldotti, A. Molinari, F.I. Danilov, A.B. Velichenko, J. Electroanal. Chem. 534 (2002) 1.
[46] P.E. Pascoe, A.H. Anbuky, J. Power Sources 111 (2002) 304.
[47] C.P. de Oliveira, M.C. Lopes, J. Power Sources 138 (2004) 294.
[48] H. Nguyen Cong, P. Chartier, J. Power Sources 13 (1984) 223.
[49] I. Petersson, B. Berghult, E. Ahlberg, J. Power Sources 74 (1998) 68.
[50] D. Pavlov, A. Dakhouche, T. Rogachev, J. Appl. Electrochem. 27 (1997) 720.
[51] K. Asai, M. Tsubota, K. Yonezu, K. Ando, J. Power Sources 7 (1981/82) 73.
[52] I. Petersson, E. Ahlberg, J. Power Sources 91 (2000) 137.
[53] L. Narasimhan, P. Raj, Z. Hussain, J. Power Sources 78 (1999) 214.
[54] C.V. D'Alkaine, A. Carubelli, M.C. Lopes, J. Power Sources 64 (1997) 111.
[55] C.V. D'Alkaine, R.P. Impinisi, A. Carubelli, J. Power Sources 113 (2003) 293.
[56] R.J. Ball, R. Kurian, R. Evans, R. Stevens, J. Power Sources 111 (2002) 23.
[57] R.J. Ball, R. Kurian, R. Evans, R. Stevens, J. Power Sources 109 (2002) 189.
[58] D. Devilliers, M.T. Dinh Thi, E. Mahé, V. Dauriac, N. Lequeux, J. Electroanal. Chem. 573 (2004) 227.
[59] D. Pavlov, J. Electroanal. Chem. 118 (1981) 167.
[60] M. Cao, C. Hu, G. Peng, Y. Qi, E. Wang, J. Am. Chem. Soc. 125 (2003) 4982.
[61] N. Vatistas, S. Cristofaro, Electrochem. Commun. 2 (2000) 334.
[62] V. Rammelt, G. Reinhard, Electrochim. Acta 35 (1990) 1045.
[63] F. Mansfeld, L.T. Han, C.C. Lee, G. Zhang, Electrochim. Acta 43 (1998) 2933.
[64] C.M.A. Brett, A.M. Olivera Brett, Electrochemistry Principles, Methods and Applications, Oxford University Press, 1993.
[65] R.J. Hill, J. Power Sources 25 (1989) 313.
[66] S.M. Caulder, J.S. Murday, A.C. Simon, J. Electrochem. Soc. 120 (1973) 1515.
[67] S.M. Caulder, A.C. Simon, J. Electrochem. Soc. 121 (1974) 1546.
[68] S.M. Caulder, A.C. Simon, J.T. Stemmle, J. Electrochem. Soc. I22 (1975) 461–466;
S.M. Caulder, A.C. Simon, J.T. Stemmle, J. Electrochem. Soc. 122 (1975) 1640–1648.
[69] R.J. Hill, A.M. Jessel, J. Electrochem. Soc. 134 (1987) 1326.